Astronomy & Astrophysics manuscript no. ryden˙astroph
October 2, 2009

Chemical abundances for 11 bulge stars from high-resolution, near-IR spectra.⋆

N. Ryde[1,2], B. Gustafsson[2], B. Edvardsson[2], J. Meléndez[3], A. Alves-Brito[4], M. Asplund[5], B. Barbuy[4], V. Hill[6], H. U. Käufl[7], D. Minniti[8,9], S. Ortolani[10], A. Renzini[11], and M. Zoccali[8]

[1] Lund Observatory, Box 43, SE-221 00 Lund, Sweden
[2] Department of Physics and Astronomy, Uppsala University, Box 515, SE-751 20 Uppsala, Sweden
[3] Centro de Astrofisica da Universidade do Porto, Rua das Estrelas, 4150-762 Porto, Portugal
[4] Department of Astronomy, University of São Paulo, IAG, Rua do Matão 1226, São Paulo 05508-900, Brazil
[5] Max-Planck-Institut für Astrophysik, Karl-Schwarzschild-Str. 1, D-85748 Garching
[6] Boulevard de l'Observatoire, B.P. 4229, F-06304 NICE Cedex 4
[7] ESO, Karl-Schwarzschild-Str. 2, 85748 Garching, Germany
[8] Department of Astronomy and Astrophysics, Universidad Catolica de Chile, Casilla 306, Santiago 22, Chile
[9] Vatican Observatory, V00120 Vatican City State, Italy
[10] Department of Astronomy, Padova University, Vicolo dell'Osservatorio 2, I-35122 Padova, Italy
[11] Osservatorio Astronomico di Padova, Vicolo dell'Osservatorio 5, I-35122 Padova, Italy
e-mail: ryde@astro.lu.se

Received ; accepted

ABSTRACT

Context. It is debated whether the Milky Way bulge has the characteristics of a classical bulge sooner than those of a pseudobulge. Detailed abundance studies of bulge stars is a key to investigate the origin, history, and classification of the bulge. These studies can give constraints on the star-formation history, initial mass-function, and trace differences in stellar populations. Not many such studies have been made due to the large distance and large variable visual extinction along the line-of-sight towards the bulge. Therefore, near-IR investigations are to be preferred.

Aims. The aim is to add to the discussion on the origin of the bulge and to study detailed abundances determined from near-IR spectra for bulge giants already investigated with optical spectra, the latter also providing the stellar parameters which are very significant for the results of the present study. Especially, the important CNO elements are better determined in the near-IR. Oxygen and other α elements are important for the investigation of the star-formation history. The C and N abundances are important for determining the evolutionary stage of the giants but also the origin of C in the bulge.

Methods. High-resolution, near-infrared spectra in the H band are recorded using the CRIRES spectrometer on the *Very Large Telescope*. The CNO abundances can all be determined from the numerous molecular lines in the wavelength range observed. Abundances of the α elements Si, S, and Ti are also determined from the near-IR spectra.

Results. [O/Fe], [Si/Fe] and [S/Fe] are enhanced up to metallicities of at least [Fe/H]=−0.3, after which they decline. This suggests that the Milky Way bulge experienced a rapid and early star-formation history like that of a classical bulge. However, a similarity between the bulge trend and the trend of the local thick disk seems present. Such a similarity could suggest that the bulge has a pseudobulge origin. The C and N abundances suggest that our giants are first-ascent red-giants or clump stars, suggesting that the measured oxygen abundances are those the stars were born with. Our [C/Fe] trend does not show any increase with [Fe/H] which could have been expected if W-R stars have contributed substantially to the C abundances. No "cosmic scatter" can be traced around our observed abundance trends; the scatter found is expected, given the observational uncertainties.

Key words. stars: abundances, Galaxy: bulge, infrared: stars

1. Introduction

One great unsolved question in cosmology is how galaxies formed and acquired their stellar populations (see for instance Renzini, 2006). Two scenarios have been traditionally entertained for the formation of bulges, with one lead-

Send offprint requests to: N. Ryde

⋆ Based on observations collected at the European Southern Observatory, Chile (ESO Programme 079.B-0338(A))

ing to "classical" bulges, whereby they form from merger-driven starbursts, and another leading to "pseudobulges" that would result from the "secular", dynamical evolution of disks (Kormendy and Kennicutt, 2004). In the classical bulge scenario most stars originate in a short phase of star formation when the universe was only a few Gyr old, and bulge formation may precede that of the disk, that could be acquired later. Instead, in the so-called "pseudobulges" stars form in the disk, over an extended period of time, and the bulge results from the secular evolution of the disk driven by the development of a bar. Thus, one expects classical bulges to be made almost exclusively of old stars, while stars in pseudobulges would have an age spread comparable to the Hubble time.

The bulges of early-type spirals (Sa and Sb) are generally considered to be "classical", while pseudobulges are thought to inhabit preferentially late-type spirals (Sc and Sd). The Sbc Milky Way (MW) galaxy sits morphologically on the borderline, hence it is no surprise that the origin of its bulge is currently a matter of debate. What is especially puzzling with the MW bulge is that it looks dynamically "pseudo" (with its boxy, peanut-shaped bar, Kormendy & Kennicutt 2004), while its stellar content is just what one expects for a "classical" bulge. Indeed, deep color-magnitude diagrams (CMD) of the MW bulge show no detectable trace of stellar populations younger than $\sim$ 10 Gyr (Ortolani et al. 1995; Zoccali et al. 2003), a conclusion for which compelling evidence has been recently provided by the deep CMD obtained with HST for a proper-motion selected sample of bulge stars (Clarkson et al., 2008).

Such a sharp distinction between these two scenarios of bulge formation has been called into question recently: observations of disk galaxies at redshift $\sim$ 2 (lookback time $\sim$ 10 Gyr) have indeed revealed that such early disks have radically different physical properties compared to local disks of similar mass. The early disks are characterized by much higher velocity dispersion and gas fraction, and harbor massive, highly star-forming clumps (Genzel et al., 2006; Förster Schreiber et al., 2009). Thus, dynamical instabilities in such early disks would occur with much shorter timescales (few 10^8 years) compared to local disks, with a secular, but fast evolution of such disks resulting in the early formation of a bulge (Genzel et al., 2008). In parallel to observations, theories have also envisaged an early production of bulges via the migration and central coalescence of gas-rich clumps in high-redshift disks (e.g., Immeli et al., 2004; Elmegreen and Elmegreen, 2005; Carollo et al., 2007; Bournaud and Elmegreen, 2009).

Determinations of detailed chemical compositions are key data for studies of the origin and evolution of stellar populations, since they carry characteristic signatures of the objects that enrich the interstellar gas. Abundance ratios are sensitive to the time-scales of star formation, to the initial mass function (IMF), and may disclose relations between different stellar groups, since different elements are synthesized by different processes and stars. For the bulge, a high ratio of α-element abundances relative to Fe is observed, suggesting that the star-formation period was early and very short (Lecureur et al., 2007; Fulbright et al., 2007) and that the bulge formed more rapidly than the thin, and perhaps even the thick galactic disk (McWilliam et al., 2008).

With stellar abundance ratios carrying such a *genetic* information on the origin of different stellar populations, Zoccali et al. (2006) compared the [O/Fe] ratios of bulge stars with those of thin disk and thick disk stars from Bensby et al. (2004). Finding bulge ratios systematically higher than disk ones, Zoccali et al. argued against the bulge having been appreciably contaminated by the migration of thick disk stars analogous to those in the solar neighborhood. A similar consideration was put forward by Lecureur et al. (2007), based on the much higher values of their [Na/Fe], [Mg/Fe] and [Al/Fe] ratios in bulge stars compared to those in thin and thick disk stars from Bensby et al. (2005), Bensby and Feltzing (2006), and Reddy et al. (2006). However, differences in abundance ratios may be also due to differences in systematic errors when the abundance analysis is done by different groups, using different data and methods. For example, cool giants with crowded spectra are prone to many systematic uncertainties (see, for instance, Santos et al., 2009) and comparing abundances derived from metal-rich, cool giants to those of solar-type dwarfs could be uncertain due to relative systematics.

In this context, Meléndez et al. (2008) carried on an homogeneous abundance analysis of bulge, thick disk and thin disk giant stars, confirming the [O/Fe] trend found by Zoccali et al. (2006) for bulge stars, but finding [O/Fe] ratios for thick disk stars much higher than those derived by Bensby et al. (2004). Thus, in the study by Meléndez et al. the high thick-disk [O/Fe]-ratios appear to be indistinguishable from those of the bulge. This similarity of [O/Fe] ratios between bulge and thick disk stars weakens the conclusion of Zoccali et al. (2006) about the genetic difference between the bulge and the thick disk, although it remains to be seen whether this similarity holds also for other [α/Fe] ratios, that appear so different in Lecureur et al. (2007). If thick disk and bulge giants follow the same [O/Fe] vs [Fe/H] relation the inference would be that both have formed "rapidly". The properties of z$\sim$ 2 disks, with their high velocity dispersion and high star formation rate, suggest that what we see there is thick-disk formation.

Determination of abundances for a large sample of red giant stars and planetary nebulae (cf. Chiappini et al., 2009) in various bulge fields as well as in the inner galactic disk will obviously provide a most powerful method to constrain the chemical evolution and models of the bulge (Matteucci and Romano, 1999; Silk and Wyse, 1993). A way to achieve this is by high-resolution, near-IR spectroscopy of red-giant stars. In the IR, the obscuration in the direction of the bulge is considerably reduced, offering us the opportunity to go to heavily reddened regions. Furthermore, near-IR spectra suffer much less from line blending than spectra at optical wavelengths, which makes it possible to safely trace the continuum and avoid abundance criteria marred with blending lines, so important in abundance analysis. Moreover, only the IR offers, even within a small wavelength range, all indicators necessary to accurately determine the CNO abundances by the simultaneous observations of many clean CO, CN and OH lines. Here, we present the first data from our VLT/CRIRES programme in which we systematically study stellar abundance ratios from different parts of the

Table 1. Account of our observations.

Star[a]	R.A. (J2000)	Dec. (J2000)	H	$t^b_{\rm integration}$ [s]	S/N
B3-b1	18 08 15.8	-25 42 10	11.3	2400	60
B3-b7	18 09 16.9	-25 49 28	11.6	4200	40
B3-b8	18 08 24.6	-25 48 44	11.9	3840	90
BW-b6	18 04 45.1	-29 48 52	11.9	3840	60
BW-f6	18 04 56.1	-29 48 59	12.0	4800	90
B6-f1	18 10 04.5	-31 41 45	11.9	1920	50
B6-b8	18 09 55.9	-31 45 46	11.9	3840	60
B6-f7	18 03 52.3	-31 46 42	11.9	1920	50
Arp 4203	18 03 23.6	-30 01 59	9.2	200	80
Arp 4329	18 03 28.4	-29 58 42	11.1	1800	95
Arp 1322	18 03 49.4	-30 01 54	10.3	600	110

[a] The designation of the stars is adopted from Lecureur et al. (2007).

[b] The total integration times are given by NDIT × DIT × NEXP × NABCYCLES × 2, see the CRIRES User's manual at http://www.eso.org/sci/facilities/paranal/instruments/crires/doc/

Galactic bulge. In particular, we have aimed at the key elements C, N, and O, but also include some α elements.

2. Observations

In the *VLT* programme 'Unveiling the secrets of the Galactic bulge: an infrared spectroscopic study of bulge giants' we have as yet observed 8 bulge stars in the *H band* with the CRIRES spectrometer (Käufl et al., 2004; Moorwood, 2005; Käufl et al., 2006). CRIRES is a cryogenic echelle spectrograph designed for high spectral resolution, near-infrared observations. Adaptive Optics (MACAO - Multi-Applications Curvature Adaptive Optics) was used, enhancing the spatial resolution and the signal-to-noise ratio. The Adaptive Optics, which is only feasible and available in the near-IR, has also the advantage to reject diffuse starlight which may affect observations in regions of high star density.

The giants we have observed are chosen from the optical investigation of Lecureur et al. (2007), sampling three fields towards the Galactic bulge; at (l, b)= (0^o,-6^o), (1^o,-4^o) [Baade's Window], and (5^o,-3^o) [Globular Cluster NGC6553]. Lecureur et al. (2007) analysed UVES/FLAMES spectra and derived abundances, but the determinations for the important C, N, and O elements need improvement. The K giants are chosen half-way up along the red-giant branch (RGB), with 4000 K $\leq T_{\rm eff} \leq$ 4500 K, a range where the molecular diagnostics are optimal and where adequate S/N ratios can be achieved. Spectra of these stars may be modelled more successfully than those of stars higher up along the RGB, which makes the abundance analysis much more reliable. The surface compositions are characteristic of the gas from which the stars once formed, with the exception of changes in C and N, the sums of which are, however, expected to be left unaltered by dredge-up of CN-processed material from the stellar interiors. The H magnitudes and the total integration times (ranging from 32 to 80 minutes) for each programme star are given in Table 1. Our observations were performed during a period from May 2007 to October 2008.

Zoccali et al. (2008) determined an iron-abundance distribution for the bulge from approximately 800 K giants (including the ones we have observed) in four fields toward the bulge with the VLT/FLAMES in the GIRAFFE mode at $R = 20,000$. They find a clear gradient going to lower latitudes. The iron distribution functions of the stars in the different fields range mainly from $-1.5 <$ [Fe/H] $< +0.5$, but the peaks of the distributions lie at lower [Fe/H] for lower latitudes. All our eleven stars from three fields in the bulge have less than solar metallicity.

The projected slit width on the sky was $0.30 \pm 0.01''$ yielding a spectral resolution of $R \sim \lambda/\Delta\lambda = 70,000$ with 3.0 pixels per spectral resolution element.[1] This will allow us to resolve blends, define the continuum, and adequately take care of telluric lines. In principle, with ideal adaptive optics and perfect image quality the true effective defining entrance slit would be the diffraction limited image of the star itself as delivered to the instrument.[2] CRIRES, however, does not reach this limit due to the finite pixel size ($\sim 1500\,{\rm ms}^{-1}$ equivalent) and the limited optical quality of the internal optics, mostly due to the relatively large ZnSe pre-dispersion prism. Indeed, the optical quality of the complete pre-disperser is just marginally sufficient for the nominal resolution of $R = 100,000$. In addition, at the wavelength of interest here, the adaptive optics does not deliver diffraction limited images, but only a core with a halo. This implies that the finite slit width rules the effective spectral resolution. During the commissioning of the CRIRES-MACAO system the effective point-spread function was analyzed in great detail, and even in the K-band under perfect conditions the enslitted energy fraction for the nominal 0.2" slit never exceeded 60%, while with fainter stars and normal seeing conditions this fraction was more like 40-50%. For more details see Table 1 in Paufique et al. (2006).

The wavelength range expected from the '$36/-1/i$'-setting of CRIRES (i.e. in Echelle order 36) was 1539.3 – 1565.4 nm over the detector arrays, consisting of a mosaic of four Aladdin III InSb arrays in the focal plane. At order 36 the blaze function of the grating limits the throughput for detector arrays #1 and #4 markedly. We, therefore, concentrated our analysis on detector arrays #2 and #3. Data for the first and fourth detector arrays were used to check abundances when possible. This is, nevertheless, an improvement in wavelength coverage compared with the Phoenix spectrometer (Hinkle et al., 1998) at the Gemini telescope, an instrument that inspired the design of

[1] The scale in dispersion direction is 0.10 ″/pixel at the center of the order and 0.095″ – 0.108″/pixel over the focal plane from the long wavelength-side to the short. In the spatial direction the scale is 0.087 ″/pixel. This change of scale is due to the change of the beam-diameter induced by the off-axis reflection at the Echelle grating which produces an anamorphism.

[2] In such a case the spectrograph entrance slit would only be a technicality to reduce the background and to establish geometric alignment, here mostly compensating pointing errors.

Table 2. Stellar parameters for the model atmospheres of our programme stars given as $T_{\rm eff}/\log g/[{\rm Fe/H}]/\xi_{\rm micro}$.

Star	Stellar parameters[a] determined by		Stellar model parameters adopted in this paper		
	Lecureur et al. (2007)	M. Zoccali (2009), private comm. see also Zoccali et al. (2008)	$T_{\rm eff}/\log g/$ [Fe/H] $/\xi_{\rm micro}$	[α/Fe]	$\xi^b_{\rm macro}$ FWHM in km s^{-1}
B3-b1	4300/1.7/ − 0.78/1.5	4400/1.7/ − 0.60/1.3	4365/2.0/ − 0.73/1.5	+0.3	5.0
B3-b7	4400/1.9/ + 0.20/1.3	4350/1.6/ + 0.21/1.2	4310/2.1/ + 0.06/1.6	+0.08	4.8
B3-b8	4400/1.8/ − 0.62/1.4	4350/1.7/ − 0.65/1.4	4250/1.5/ − 0.69/1.4	+0.3	4.8
BW-b6	4200/1.7/ − 0.25/1.3	4450/1.9/ − 0.20/1.4	4340/2.2/ − 0.16/1.5	+0.15	4.3
BW-f6	4100/1.7/ − 0.21/1.5	4400/1.8/ − 0.23/1.6	4150/1.5/ − 0.31/1.6	+0.2	5.0
B6-f1	4200/1.6/ − 0.01/1.5	4250/1.9/ − 0.08/1.5	4030/1.3/ − 0.08/1.5	+0.1	5.3
B6-b8	4100/1.6/ + 0.03/1.3	4250/1.8/ − 0.06/1.4	3985/1.1/ − 0.14/1.3	+0.1	5.7
B6-f7	4300/1.7/ − 0.42/1.6	4450/1.8/ − 0.27/1.5	4315/1.9/ − 0.34/1.6	+0.2	4.8
	Stellar parameters[a] determined by		Stellar model parameters adopted in this paper		
	Fulbright et al. (2007) & used by Ryde et al. (2009)		$T_{\rm eff}/\log g/$ [Fe/H] $/\xi_{\rm micro}$	[α/Fe]	$\xi^b_{\rm macro}$ FWHM in km s^{-1}
Arp4203	3902/0.5/ − 1.25/1.9		3815/0.35/ − 1.25/1.8	+0.35	6.2
Arp4329	4197/1.3/ − 0.90/1.5		4153/1.15/ − 1.02/1.5	+0.35	5.8
Arp1322	4106/0.9/ − 0.23/1.6		4250/1.5/ − 0.16/1.5	+0.15	6.2
Arcturus	4290/1.5/ − 0.5/1.7		4280/1.7/ − 0.53/1.7	+0.3	3.7

[a] The stellar parameters are given as the effective temperature, $T_{\rm eff}$, in K, the logarithmic surface gravity, $\log g$, in cgs units, and the microturbulence, $\xi_{\rm micro}$, i

[b] The macroturbulence is given as the FWHM used in the final convolution of the synthetic spectra fitted to include both effects of stellar macroturbulence and

the CRIRES spectrometer, with a total wavelength range that corresponds to approximately one of CRIRES's detector arrays ($\Delta\lambda/\lambda = 0.5\%$). It should be noted that there are small gaps of approximately 2 nm between the spectra on the detector arrays.

The approximate signal-to-noise ratios (S/N) per pixel of the observed spectra at 1554.8 nm (a well chosen continuum region in the third detector array) are also given in Table 1. The S/N per resolution element is close to a factor of 2 larger. The S/N is difficult to measure since the many lines make it difficult to find a large enough region of continuum from which to estimate it. The numbers given here are indicative. The S/N varies by a factor of two between the detector arrays, mainly due to the blaze function. The S/N for the third detector array increases with wavelength from 90 to 110% of the S/N at the reference wavelength. For the second detector the S/N varies linearly with wavelength from approximately 70% to 100% of the S/N at the reference wavelength of the standard setting, here chosen to be at 1557.3 nm.

The observed data were reduced with the ESO standard pipe-line reduction package. The CRIRES pipeline is based on the general and coherent approach by ESO using common routines, also employed in other instruments (Ballester et al., 2006). The wavelength solution is based on a physical model approach for CRIRES (Kerber et al., 2008a) using telluric emission lines and the new infrared line catalog for ThAr hollow arc lamps (Kerber et al., 2008b). For the extraction of one-dimensional spectra the data taken for different positions of the star along the slit (resulting from nodding and dithering) are corrected in the usual way for glitches and bad pixels and then rebinned in wavelength space before co-addition. The final extraction is based on the "optimal extraction" method which preserves the flux without sacrificing S/N-ratio. [3]

In addition to these eight giants, we have reanalysed the three bulge giants presented in Ryde et al. (2009). These were also observed with CRIRES, during its science verification, on 12 August 2006. The H magnitudes and the total integration times are given in Table 1. The observations and data are similar to those of our new eight stars, although they were observed at $R = 50,000$ and processed with routines in the reduction package `IRAF` (Tody, 1993)[4], in order to retrieve one-dimensional, continuum normalised, and wavelength calibrated stellar spectra.

3. Analysis

We analyze our spectra by modelling the stellar atmosphere and calculating synthetic spectra for the observed spectral region. These are thereafter convolved in order to fit the shapes and widths of the lines, including the stellar macroturbulence and instrumental broadening. We then derive elemental abundances

[3] Full details of the pipeline can be found under http://www.eso.org/observing/dfo/quality/CRIRES/pipeline/pipe_reduc.html

[4] IRAF is distributed by the National Optical Astronomy Observatory, which is operated by the Association of Universities for Research in Astronomy (AURA) under cooperative agreement with the National Science Foundation.

by fitting the synthetic to the observed spectra. In this section we will discuss the model atmospheres, the stellar parameters including their uncertainties, and the spectrum synthesis.

3.1. Model atmospheres

We have calculated model atmospheres with the MARCS code (Gustafsson et al., 2008) after adopting the stellar effective temperature, logarithmic surface gravity, metallicity, microturbulence, and [α/Fe] enhancement for the model of each of our stars (see Table 2, column 4). The MARCS standard models are hydrostatic and are computed on the assumptions of Local Thermodynamic Equilibrium (LTE), chemical equilibrium, homogeneous spherically-symmetric stratification (in our case with $M_{\rm star} = 0.8\,{\rm M}_{\odot}$), and the conservation of the total flux (radiative plus convective; the convective flux being computed using the local mixing length recipe). The radiation field used in the model generation is calculated with absorption from atoms and molecules by opacity sampling at approximately 100 000 wavelength points over the wavelength range 1300 Å–20 μm. The models are calculated with 56 depth points from a Rosseland optical depth of $\log\tau_{\rm Ross} = 2.0$ out to $\log\tau_{\rm Ross} = -5.0$. Data on absorption by atomic species are collected from the VALD database (Piskunov et al., 1995) and Kurucz and other authors (for details, see Gustafsson et al., 2008). The molecular-line opacity of CO, CN, CH, OH, NH, TiO, VO, ZrO, H_2O, FeH, CaH, C_2, MgH, SiH, and SiO is included and up-to-date dissociation energies and partition functions are used. It should be noted that, for our targeted elements, we iterate and specify these abundances for each new iteration of the model atmosphere calculation, in order to be self-consistent.

The atomic line absorption files used in a MARCS model calculation are pre-calculated in a grid. Those used for our models are thus files with general metallicities closest to the metallicity of the stars. The grid is given in steps of Δ[Fe/H] = 0.25 dex in the relevant metallicity range. For stars with [Fe/H] < 0.0, [α/Fe] can be solar or $\alpha-$enriched by up to 0.4 dex. For more metal-rich stars the abundance ratios are solar. Microturbulence parameters of 1 or 5 km s^{-1} were used in the model calculations.

3.2. Fundamental stellar parameters and their uncertainties.

3.2.1. Deriving the fundamental parameters for our stars

The fundamental stellar parameters, i.e $T_{\rm eff}$, $\log g$, [Fe/H], and $\xi_{\rm micro}$, are needed as input for the model photosphere and spectrum synthesis. Optical Fe I and Fe II equivalent widths were used to obtain spectroscopic surface gravities and effective temperatures by requiring a relative ionization and excitation equilibrium with respect to a set of standard bright giants (see Meléndez et al., 2008). The iron line list was carefully chosen to avoid significant blends in K giants (Alves-Brito et al. 2009, in preparation), and is an extension of the line list already presented in Hekker and Meléndez (2007). This is the same scale as used by Meléndez et al. (2008), which means that the stellar parameters for our stars are on the same scale as those of well-studied nearby giants, which ultimately have effective temperatures determined from the Infrared Flux Method temperature scale of Ramírez and Meléndez (2005a,b) and surface gravities based on absolute magnitudes as determined from Hipparcos parallaxes and adopting stellar masses from isochrones.

The equivalent widths (W_λ) of the iron lines for our new CRIRES stars were taken from Lecureur et al. (2007), who obtained automatic W_λ measurements from spectra observed with VLT/FLAMES in the UVES mode, providing a spectral resolution of $R = 45,000$. They used the DAOSPEC code which is described in Stetson and Pancino (2008). For one star, B6-b8, (which can be considered one of the most difficult cases, the star being cool and metal-rich) we also measured the equivalent widths manually.

The microturbulence, $\xi_{\rm micro}$, was obtained by requiring that the derived Fe I abundances are independent of line strengths. This procedure also yields the iron abundances. The [α/Fe] used in our models are based on our preliminary optical analysis of different α-elements in bulge stars (Alves-Brito et al. 2009, in preparation), and so it is based in a preliminary mean bulge relationship between [α/Fe] and [Fe/H].

Our new stellar parameters for our bulge stars, including the three stars from Ryde et al. (2009), and our reference star Arcturus, are given in Table 2. In the table we also give the [α/Fe] values that we use in the determination of the parameters and later adopt in the model calculations. The earlier determinations of the stellar parameters for these stars from the literature are also given in the table, namely those of Lecureur et al. (2007), the updated parameters based on UVES data as described in Zoccali et al. (2008), and finally Fulbright et al. (2006), the latter also used by Ryde et al. (2009). The differences in the stellar parameters, sometimes quite large, are mainly caused by the different methods applied in the different stellar parameter determinations. For instance, the different line sets used and our relative ionization-equilibrium constraint to obtain the surface gravities, can cause differences. The different values illustrate the general uncertainty, in particular the difficulties in determining the fundamental parameters from the equivalent widths observed with UVES/FLAMES (Lecureur et al., 2007). Our new effective temperatures are systematically cooler (on average by 159 K) than the updated parameters based on the UVES data, as described in Zoccali et al. (2008). For the three stars from Fulbright et al. (2006) the differences go both ways with a maximum of 144 K.

For the stars from Ryde et al. (2009), which we analyse here too, we have redetermined the fundamental parameters based on the same scale as that used for other stars presented here. We have also redetermined the fundamental parameters for our reference star Arcturus (α Boo) in the same fashion. The new parameters for these stars are given in the lower part of Table 2. The changes in the derived C, N, and O abundances for these stars compared with those derived by Ryde et al. (2009) agree with what is expected from the sensitivities of these abundances to the stellar parameters, and keeping in mind that different solar C, N, and O values are used in our paper compared to Ryde et al. (2009).

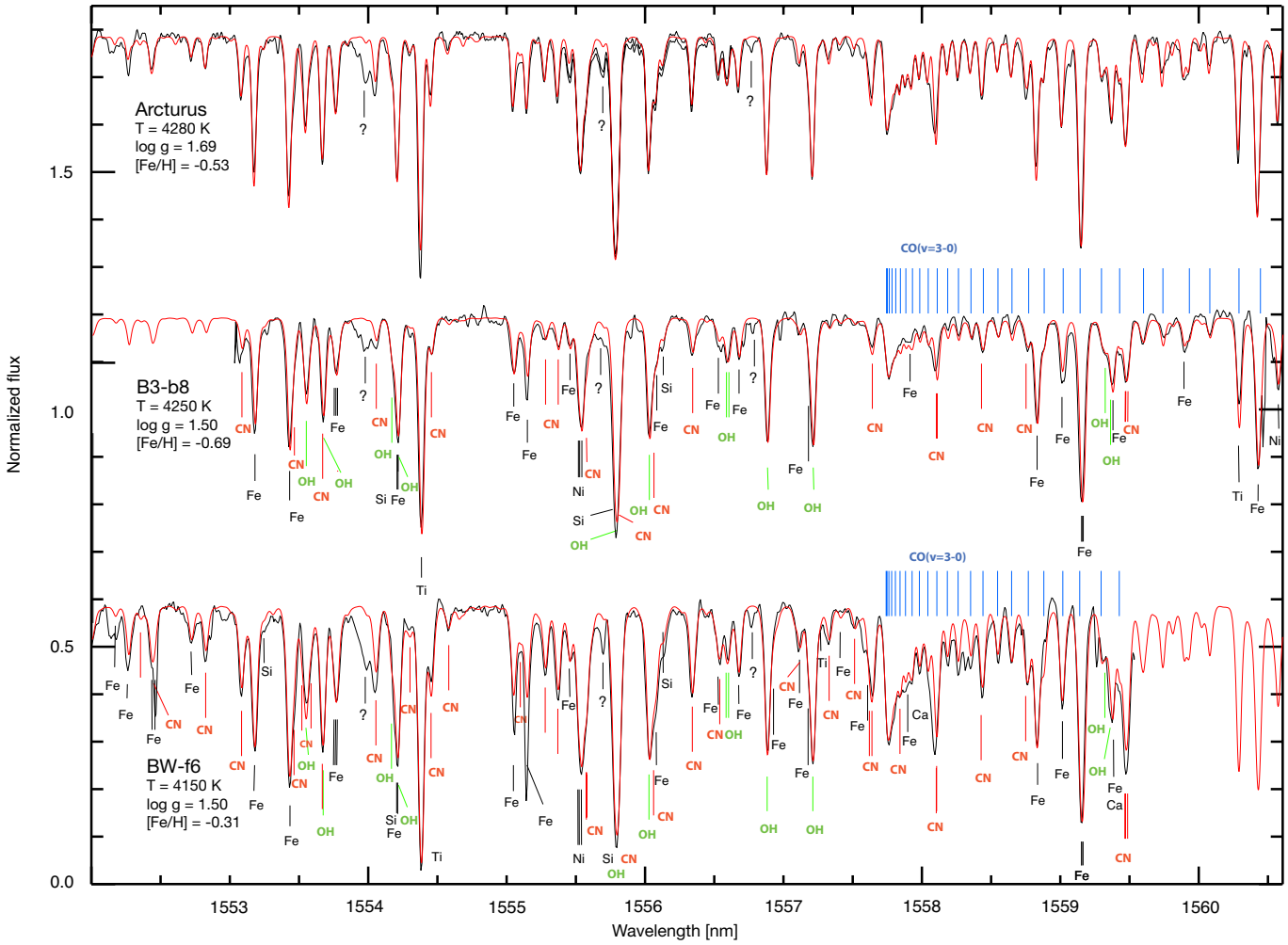

Fig. 1. Sections of the observed CRIRES spectra of two of our bulge giants are shown with full, black lines. The observations are wavelength-shifted to laboratory wavelengths in order to enable a direct comparison between the different stellar spectra. Therefore, our observed spectra cover slightly different wavelength ranges. For comparison, the Arcturus atlas spectrum (Hinkle et al., 1995b) is also shown. The parts of the spectra which have the highest signal-to-noise ratios are shown. From these parts the C, N, and O elements can be determined. Our best synthetic spectra is shown in red. All synthetic lines which are deeper than 0.97 of the continuum are identified. A few features are not identified in the Arcturus spectrum and are labeled with question marks. These features also show up in the bulge-star spectra. A few lines in BW-f6 is conspicuously stronger than expected. They are probably affected by cosmic rays in the detector array.

It would be preferable to obtain accurate effective temperatures directly from our IR spectra because of the substantial extinction towards the bulge in the visual wavelength region. This is, however, a difficult task. Although we are exploring the use of other infrared regions to improve the determination of stellar parameters, the current infrared spectrographs available to us in 8m-class telescopes only cover a narrow region, therefore requiring considerable amounts of telescope time to improve the stellar parameters based solely on infrared data. Furthermore, the limited ranges in excitation energy for lines of various molecular species limit their use for $T_{\rm eff}$ determination. Effective-temperature sensitive features are particularly the OH molecular lines which are used for oxygen abundance determinations. Other lines are only weakly sensitive. Carbon, which appears in numerous lines of four different species, should in principle be useful for $T_{\rm eff}$ determination. Our tests show, however, that for a 100 K increase in $T_{\rm eff}$ and for fundamental parameters which are typical of our targets the high-excitation C I lines become only slightly stronger, the CN lines stay unchanged, the CO lines become slightly weaker, and the C_2 lines stay almost unchanged. High S/N spectra or large wavelength regions would therefore have to be observed for the purpose. In the near future we, therefore, intend to rely on spectroscopic equilibrium based on optical FeI and FeII lines. Besides the current work of Alves-Brito et al. to define the zero-points of the spectroscopic stellar parameters, we are currently acquiring more high resolution optical data of bright K giants, which will allow us to further improve our stellar parameter scale. We are also starting simulations that will allow us to estimate realistic uncertainties in the atmospheric parameters of cool giants (Meléndez, Coelho, Alves-Brito, in preparation).

3.2.2. Uncertainties in the fundamental parameters

Our $T_{\rm eff}$ values are uncertain, limited by the uncertainties in the W_λ measurements. However, the small dispersion in the [O/Fe] vs. [Fe/H] plot (Figure 2) suggests that the random errors are of the order of 75 K. This is the value we use to derive the impact of this uncertainty on the derived abundances, see Table 4. However, the uncertainty could be underestimated.

Our spectroscopic surface gravity determinations are also very uncertain with uncertainties estimated to 0.3 dex (in some cases by as much as 0.5 dex), again mainly due to the quality of the W_λ measurements of the few and weak Fe II lines but also the fact that we assume LTE in the ionization equilibrium, which might not be valid. However, our $\log g$ values more or less follow our expectations for giants with $T_{\rm eff} = 4000$ K ($\log g \sim 1.0$) and 4300 K ($\log g = 2.0$). On the other hand, these gravities locate a few of the stars at distances not compatible with the bulge (all distances lie between 4.5 and 12 kpc). Our stars are chosen from the bulge giants of Lecureur et al. (2007) which were selected to have a high probability of being bulge members. We have therefore also calculated the photometric surface gravities, using the PARAM tool (see da Silva et al., 2006), forcing the stars to lie at a distance of 8 kpc (Reid, 1993) and calculating the extinction in the same way as Lecureur et al. (2007). Our resulting gravities are given in Table 3 together with our spectroscopic ones. The $\log g$ values obtained by Zoccali et al. (and Lecureur et al.) are also determined photometrically and fall in the range 1.7 ± 0.1 dex, in good agreement with our photometric values. The main uncertainty in the photometric gravities is due to fact that the actual distances to the stars are not well known and the bulge does have an extension of a few kpc. Allowing a conservative uncertainty of ± 2 kpc in the distance of 8 kpc, we find an uncertainty in the gravities of 0.25 dex, due to the distance uncertainty only. The sensitivity of the determination of $\log g$ to the extinction and the differential reddening, of which the latter is not taken into account, is small (see Lecureur et al., 2007). The gravities based on the two methods, given in Table 3, are compatible with each other within the uncertainties, the differences being mostly < 0.3 dex, except for one case, B6-b8, which is a cool and metal-rich giant. Fortunately, in our case, whichever $\log g$ determination we assume does not make a big difference, especially for the oxygen abundance from the OH lines, as can be seen from Table 4 and Figure 2. The carbon abundance determined from the CO lines is, however, affected more, see also Figure 4. In the following discussion we have chosen to use the surface gravities determined spectroscopically.

Finally, we estimate the uncertainty in the metallicity to be, in general, of the order of 0.05 dex and in the microturbulence to be of the order of 0.25 kms^{-1}.

The changes in the fundamental parameters due only to the two different measurements of the equivalent widths (automatic DAOSPEC or manually) of the cool and metal-rich giant, B6-b8, are 20 K in the temperature, 0.16 dex in $\log g$, -0.17 dex in [Fe/H], and 0.35 km s^{-1} in the microturbulence. The differences are within our estimated total uncertainties, except for the $\xi_{\rm micro}$ and the metallicity. This star is, however, particularly cool and metal-rich which means that the iron line measurements are especially difficult for this star.

Table 3. Spectroscopically and photometrically determined surface gravities.

Star	$\log g_{\rm spec}$	$\log g_{\rm photo}$	Difference $\log g_{\rm photo} - \log g_{\rm spec}$
B3-b1	2.0	1.7	−0.3
B3-b7	2.1	1.8	−0.3
B3-b8	1.5	1.7	0.2
BW-b6	2.2	1.9	−0.3
BW-f6	1.5	1.8	0.2
B6-f1	1.3	1.6	0.3
B6-b8	1.3	1.7	0.4
B6-f7	1.9	1.8	−0.1
Arp4203	0.3	0.6	0.3
Arp4329	1.2	1.5	0.3
Arp1322	1.5	1.5	−0.0

3.3. Synthetic spectra

For the analysis of the observed spectra, we have generated synthetic spectra, calculated in spherical symmetry for our model photospheres. We sample the spectra with a resolution of $R = 600,000$. With a microturbulence velocity of $1 - 2$ km s^{-1}, this will ensure an adequate sampling. In order to fit the observed spectra, we finally convolve our synthetic spectra with a macroturbulent broadening, represented by a radial-tangential function (Gray, 1992), and fitted to include both effects of macroturbulence and instrumental profile. The final macroturbulence parameters used are given in Table 2. The code used for calculating the synthetic spectra is BSYN v. 7.06 which is based on routines from the MARCS code. Full consistency with the model atmosphere is achieved by choosing the same fundamental parameters, [α/Fe], individual abundances and in both calculations, including the molecular equilibria. A ^{12}C/^{13}C ratio of 24 (96% ^{12}C) is used for the bulge stars, and of 9 for Arcturus.

The atomic line-list used in our calculations is compiled from the VALD database (Piskunov et al., 1995) and from Meléndez and Barbuy (1999). The stellar parameters of our bulge stars resemble those of α Boo, which is therefore a good choice as a reference star. However, most of the lines used in our analysis can also be analyzed in the solar spectrum. We have, therefore, primarily checked the line list against the solar spectrum and corrected the line-strengths, if needed, by determining 'astrophysical $\log gf$-values', fitting atomic lines in synthetic solar spectra to the observed one (Livingston and Wallace, 1991). Hence, in our line list we have adjusted 96 lines based on the solar spectrum, see Table 7. The lines fitted were, among others, some Fe, Ni, Si, S and Ti lines. In addition, 4 Ti lines and 4 Si lines, which were too weak in the solar spectrum, were fitted to the α Boo spectrum from the Hinkle et al. (1995a) atlas. These 8 lines are also given in Table

7. In order to determine the astrophysical $\log gf$-values of these lines, we need to know the abundances of these elements in α Boo. Furthermore, apart from iron, Mg and Si are the most important electron donors at the continuum-forming regions, and therefore affect the line strengths through the continuous opacity (H^-_{ff}). It is therefore important to estimate the abundance of Fe and Mg also, as well as possible. Hence, the Fe, Mg, Si, and Ti abundances of our Arcturus modeling are based on the optically determined abundances derived by Fulbright et al. (2007), but taking into consideration our slightly different fundamental parameters, which, however, increased these abundances by only 0.00, 0.01, 0.03, and 0.01 dex, respectively. The other Fe, Si and Ti lines in our near-IR list, yield the same abundance for Arcturus, within a few tenth of a dex. To conclude, the line list used here is similar to the one described in Ryde et al. (2009), except that some new lines are added, a few omitted, the strengths of nine lines were adjusted slightly (less than 0.1 dex), and the strengths of 2 Ti lines (15334.84 and 15543.78 Å) and one Si line (15506.98 Å) strengths were adjusted by a larger amount. The latter three lines are all visible in the sun.

The molecular lists included are, for CO Goorvitch (1994), SiO Langhoff & Bauschlicher (1993), CH Jørgensen et al. (1996), CN Jørgensen & Larsson (1990) and Plez (1998, private communications), OH Goldman et al. (1998), and C_2 Querci et al. (1971) and Jørgensen (2001, private communications). For the molecules, the line lists were adopted as they are, leading to the following C, N, and O abundances for Arcturus from the spectra in the Arcturus atlas (Hinkle et al., 1995a): $\log\varepsilon_C = 8.08 \pm 0.11$ (from CO lines), $\log\varepsilon_N = 7.64 \pm 0.09$ (from CN lines), and $\log\varepsilon_O = 8.70 \pm 0.13$ (from OH lines), which are in excellent agreement with the values derived by Ryde et al. (2009) and by the optical work by Lecureur (2007), who derived $\log\varepsilon(C) = 7.96 \pm 0.10$, $\log\varepsilon(N) = 7.74 \pm 0.10$, and $\log\varepsilon(O) = 8.70 \pm 0.05$.

From our spectra, we have determined elemental abundances from the CO [$v = 3 - 0$] band, around 20 suitable CN lines, some 20 suitable OH [$v = 4 - 2, 3 - 1, 2 - 0$] lines, and numerous Fe I lines. Silicon can be measured from 2 or 3 lines, sulphur from 2 lines, and titanium only from 1 line, which makes the derived Ti abundance the most uncertain of the α elements. We find the best fits, line by line, by synthesizing a grid of model spectra with incremental differences of 0.05 dex in the abundance sought for and finding the best fit by visual inspection. While for the OH and CN lines, and the atomic lines, every suitable line was inspected, for the CO band the entire band was fitted. In Figure 1 we present two examples of spectra of our 8 bulge stars, namely those of B3-b8 and BW-f6. These are spectra for which we obtained the highest S/N. Only the third detector array, providing the highest S/N, is shown, but spectra from the other detector arrays were also used in the analysis. The reference spectrum of Arcturus is also shown in the Figure.

Table 4. Uncertainties in the derived abundances due to uncertainties in the stellar parameters.

	$\Delta\log\varepsilon$(C)	$\Delta\log\varepsilon$(N)	$\Delta\log\varepsilon$(O)	$\Delta\log\varepsilon$(S)
$\Delta T_{\rm eff} = +75$ K	+0.04	+0.06	+0.12	−0.05
$\Delta\log g = +0.3$ (cgs)	+0.10	−0.03	+0.00	+0.10
$\Delta\xi_{\rm micro} = +0.25\,{\rm km\,s^{-1}}$	−0.01	−0.02	−0.02	−0.00
Δ[Fe/H] = +0.05 dex	+0.02	+0.04	+0.04	+0.00
$\Delta[\alpha/{\rm H}] = +0.1$ dex	+0.03	+0.02	+0.04	+0.02

3.4. Uncertainties in the derived abundances

The propagation of uncertainties in the stellar parameters to uncertainties in the C, N, and O abundances is presented in Table 4, based on the discussion in Ryde et al. (2009). These uncertainties are derived for a typical star of our sample, namely BW-f6. The uncertainty in the [α/Fe] ratio is included but ambiguous since the different α-elements show different trends. We have adopted a general enhancement of [α/Fe] = +0.2 in the model calculations and in the calculation of the synthetic spectra. We estimate the total internal uncertainties in the derived C, N, and O abundances to be approximately $\Delta A_C = 0.11$, $\Delta A_N = 0.09$, and $\Delta A_O = 0.13$ dex. As a comparison, the standard deviations in the determinations of the C, N, and O abundances from the many observed CO, CN, and OH lines for a given model are small, less than 0.05 dex. For example, for a given star and model atmosphere, the determination of the oxygen abundances from each of the approximately 20 suitable OH lines provides a mean oxygen abundance with a standard deviation of 0.04 (line-to-line scatter) and a standard deviation of the mean of 0.01 dex. We note, however, that the error in the CNO abundances generated by errors in the fundamental parameters will correlate, according to Table 4. E.g., an underestimated effective temperature will lead to underestimated abundances of C, N, as well as O. For the α elements, here represented by sulphur, we estimate $\Delta A_S = 0.11$ dex, i.e of the same order as the molecular lines. We see, however, that the oxygen abundance suffers the largest uncertainty which is mainly due to the uncertainties in the effective temperature.

The relatively low star-to-star scatter in the [O/Fe] vs. [Fe/H] plot (see Figure 2) confirms that our error bar in the stellar parameters, especially $T_{\rm eff}$, are reasonable. Although our [O/Fe] values are sensitive to the $T_{\rm eff}$, they are not much affected by the uncertainties in $\log g$, compare Table 4 and the two panels in Figure 2. On the other hand, the oxygen abundance for seven of our stars that were derived by Zoccali et al. (2006) from the [O I] line at 6300Å is not much affected by the effective temperature but much more by the surface gravity. For instance, a change in $\log g$ of +0.3 dex yields a change in the oxygen abundances of +0.13 dex from the [O I] line (cf. ∼ 0.00 dex from the OH lines), whereas a change in the temperature of 100 K yields a change of +0.02 dex (cf. +0.16 dex from the OH lines).

Other systematic uncertainties that could affect the abundance results include those due to, for instance, the continuum placement, the model atmosphere assumptions (such as the

treatment of convection and the assumption of spherical symmetry), the uncertainties in the line strengths ($\log gf$ values), and the dissociation energies of the molecules. Furthermore, possible non-LTE effects in the line formation of both atomic and molecular lines could affect the result in a systematic way. In the future, only a full non-LTE analysis of all relevant atoms and molecules would be able to disclose the magnitude of these systematic uncertainties that our LTE analysis might be plagued by. For abundance ratios, several uncertainties partly cancel leading to smaller uncertainties. The uncertainty due to the placement of the continuum is estimated to be relatively small, less than 0.03 dex.

4. Results

In Table 5 we present our derived [C/Fe], [N/Fe], [O/Fe], [Si/Fe], [S/Fe], [Ti/Fe], and [Fe/H] for our eleven bulge giants. We also provide the derived C, N, C+N, O, and S abundances for Arcturus in addition to the Si, Ti and Fe abundances used. Our iron abundances of the bulge stars, as determined from 8 to 20 Fe-lines depending on the different S/N of the IR spectra, are systematically between 0.00 to 0.10 dex larger than the optically determined metallicity as given in Table 2, which is satisfactory. In Figure 2 we plot the [O/Fe] versus metallicity for our 11 bulge giants, together with the bulge giants from Meléndez et al. (2008). These abundance ratios were also determined from near-IR spectra and the adopted stellar parameters were on the same scales. We find enhanced values of [O/Fe]$\sim +0.4$ up to approximately [Fe/H]~ -0.3, after which they decrease. In the Figure we have especially marked the giant Arp 4203 which shows a large depletion of carbon, a large enhancement of nitrogen, and a [C+N/Fe] which is far from being solar, making this giant special. This was also noted by Fulbright et al. (2007), Meléndez et al. (2008), and Ryde et al. (2009) who concluded that the oxygen abundance in this star should probably not be used to represent the unprocessed [O/H] value for this bulge giant.

In Figure 3 we plot our derived [Si/Fe], [S/Fe], and [Ti/Fe] versus our derived metallicity. For reference we also plot the trend we estimate from our [O/Fe] vs. [Fe/H] values. The abundances of the α elements are more uncertain than our derived C, N, O, and Fe abundances since there are much fewer lines to measure. The uncertainties are therefore larger for these elements than for the C, N, O, and Fe abundances. In spite of this, we find that the [α/Fe] values are enhanced for metallicities up to at least [Fe/H]~ -0.3 after which they appear to decline. Below this metallicity [Si/Fe] and [S/Fe] are enhanced at a level of [α/Fe]$\sim +0.3$. For higher metallicities they seemingly decline and follow [O/Fe] for a given metallicity. [Ti/Fe] is generally lower for all metallicities. Our α element trends overall corroborate the [O/Fe] enhancement trend, although for [Ti/Fe] at a lower value. In this Figure we have also especially marked Arp4203.

All our stars except B3-b1 show significantly enhanced [N/Fe] values. If a star has experienced the first dredge-up, CN-cycled material is exposed at its surface. The abundances of C and N are then expected to change but their sum is left unaltered. In Table 5 we also provide the calculated [(C+N)/Fe].

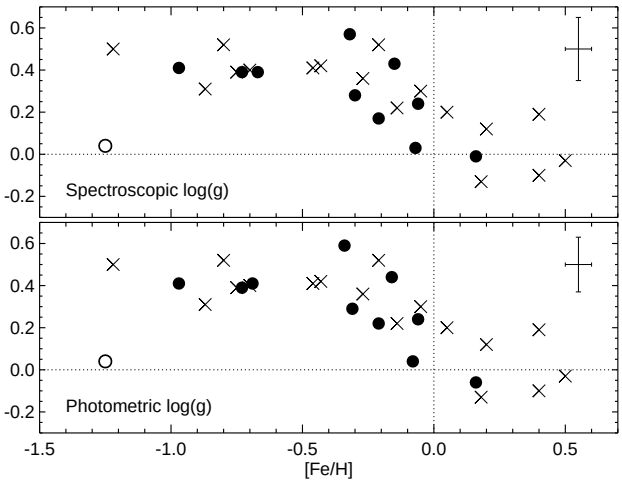

Fig. 2. Logarithmic ratios of oxygen to iron normalized on the solar value for bulge stars. Filled circles show our data from this paper, except the special giant Arp4203 which is denoted by an open circle. Crosses show the results of Meléndez et al. (2008). Typical uncertainties are indicated in the upper right corner. The upper panel shows the oxygen abundances we derive when we use our spectroscopically derived $\log g$ values for our stellar atmosphere models, whereas the lower panel shows them when we instead use our photometrically derived surface gravities.

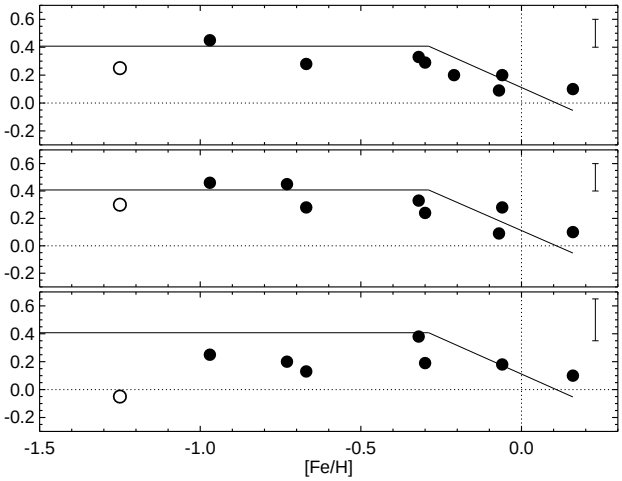

Fig. 3. Logarithmic ratios of Si, S, and Ti to iron normalized on the solar value for our bulge stars are shown with filled circles. The [O/Fe] vs. [Fe/H] trend is indicated by a full line for reference in all panels. The measured values for the special giant Arp4203 are shown with an open circle. Typical uncertainties are indicated in the upper right corners.

This is plotted in Figure 4 together with the [(C+N)/Fe] for the bulge giants from Meléndez et al. (2008). These two data sets show approximately the same pattern when it comes to the mean, standard deviation, and slope. We find a slope from a linear regression analysis for our data of $k = +0.07 \pm 0.09$ and for both sets of $k = +0.04 \pm 0.04$, i.e. both data sets are con-

Table 5. [C/Fe][a,b], [N/Fe], [(C+N)/Fe], [O/Fe], [Si/Fe], [S/Fe], [Ti/Fe], and [Fe/H] for our 11 bulge giants and Arcturus.

Star	[C/Fe]	[N/Fe]	[(C+N)/Fe]	[O/Fe]	[Si/Fe]	[S/Fe]	[Ti/Fe]	[Fe/H]
B3-b1	0.090	0.030	0.079	0.39	–	0.45	0.20	−0.73
B3-b7	−0.11	0.43	0.065	−0.01	0.10	0.10	0.10	+0.16
B3-b8	−0.10	0.21	−0.018	0.39	0.28	0.28	0.13	−0.67
BW-b6	0.13	0.27	0.16	0.43	–	–	–	−0.15
BW-f6	0.050	0.24	0.095	0.28	0.29	0.24	0.19	−0.30
B6-f1	−0.10	0.37	0.044	0.030	0.090	0.090	–	−0.070
B6-b8	0.090	0.43	0.18	0.17	0.20	–	–	−0.21
B6-f7	0.14	0.36	0.19	0.57	0.33	0.33	0.38	−0.32
Arp4203	−0.66	1.03	0.37	0.040	0.25	0.30	−0.050	−1.25
Arp4329	−0.11	0.28	0.00	0.41	0.45	0.46	0.15	−0.97
Arp1322	−0.090	0.38	0.054	0.24	0.20	0.28	0.18	−0.060
Arcturus	0.19	0.35	0.23	0.51	0.36	0.26	0.17	−0.53

[a] $[X/Fe] = \{\log\varepsilon(X) - \log\varepsilon(Fe)\}_{star} - \{\log\varepsilon(X) - \log\varepsilon(Fe)\}_{\odot}$.
[b] We have adopted the following solar abundances (Meléndez et al. 2008): $\log\varepsilon(C) = 8.42$, $\log\varepsilon(N) = 7.82$, $\log\varepsilon(O) = 8.72$, $\log\varepsilon(Fe) = 7.50$.

sistent with being sampled from a flat distribution. We further find a mean for both data sets of <[(C+N)/Fe]>= 0.08 ± 0.09 (s.d.) and an error in the mean of 0.02 dex. Thus, both data sets show a systematic enhancement in the [(C+N)/Fe] ratios and they are therefore not consistent with being at solar values for all metallicities. Given our estimated uncertainties, our stars show no cosmic scatter. More stars and higher accuracy would be needed to judge whether the off-set from solar values, the slight increase with metallicity or the curved tendency in Fig. 4 are real. We note that the highest value, apart from that of Arp4203, is that of Arcturus, with [(C+N)/Fe]=0.23.

In Figure 5 we plot C/N for our stars in the theoretical HR diagram and show how C/N varies with position in it. We see that the stars line up on the giant branch and that the C-N ratios decrease along it, as expected. Arp4203 has evolved furthest.

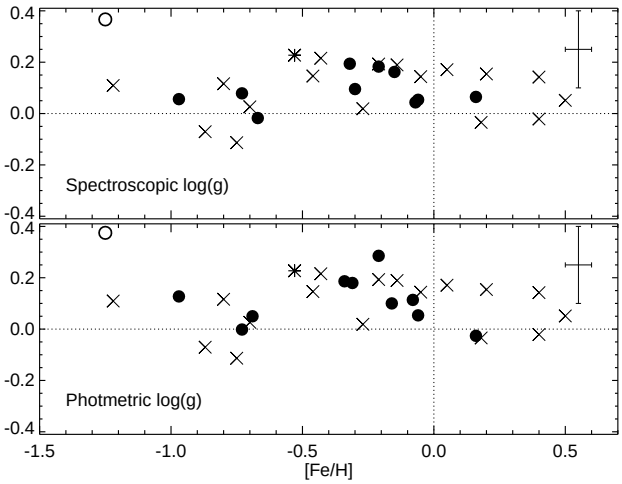

Fig. 4. Logarithmic ratios of carbon+nitrogen to iron normalized on the solar value. Our data are shown by filled circles, except Arp4203 which is shown by an open circle. Crosses show the results of Meléndez et al. (2008). The [(C+N)/Fe] value we derive for Arcturus is shown with a star. Typical uncertainties are indicated in the upper right corner. The upper panel shows the values we retrieve when assuming spectroscopically derived $\log g$ and the values presented in the lower panel assumes photometrically derived surface gravities.

5. Discussion

5.1. The [α/Fe] trends

The trends of the α elements (O, Mg, Si, S, Ca, and Ti) are of particular interest, since accurate [α/Fe] ratios in pre-AGB bulge stars will set strong constraints on the star formation history.

5.1.1. Oxygen

Our oxygen abundances show a good *general* agreement in the downward [O/Fe] vs. [Fe/H] trends with the results found by other authors. However, differences exist between these. In Figure 6 we plot the [O/Fe] trends for the bulge stars based on analyses of near-IR spectra. These are, in addition to our new results, values from Cunha and Smith (2006), Rich and Origlia (2005), Meléndez et al. (2008), and Ryde et al. (2009). The [O/Fe] vs. [Fe/H] trend of Rich and Origlia (2005) is moved upwards by 0.11 dex to adjust to the authors' assumed solar oxygen abundance of 8.83 compared to our value of 8.72. It is a bit risky to quantify the similarities of the different trends due to the small number of stars, but assuming a constant [O/Fe] vs. [Fe/H] up to a metallicity of [Fe/H]= −0.3, and assuming a constant slope thereafter up to [Fe/H]~ +0.4, we find an agreement in the slope of our data ($k = -1.0 \pm 0.3$)

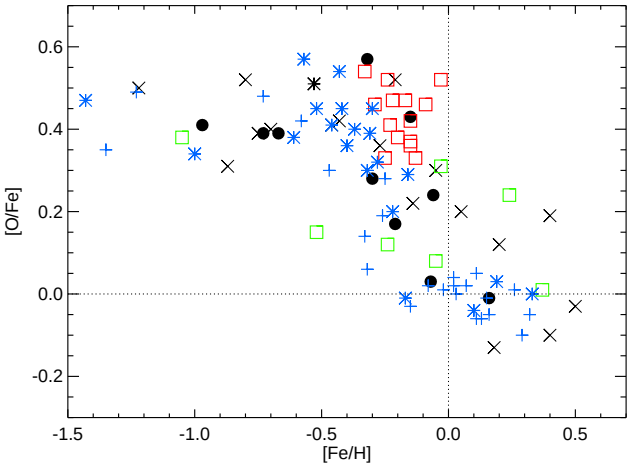

Fig. 6. Logarithmic ratios of oxygen to iron normalized on the solar value. The oxygen abundances are here all determined from near-IR spectra. Filled circles show our data from this paper, except that of Arp4203. Arcturus at [Fe/H]= −0.53 is indicated with a black star at [O/Fe]=0.51, in agreement with that of Lecureur (2007). Crosses show the results of Meléndez et al. (2008), green squares represent the abundances determined by Cunha and Smith (2006), and red squares the data from Rich and Origlia (2005). The blue star and plus signs represent thick disk and thin disk giants, respectively, from Meléndez et al. (2008).

Fig. 5. C/N ratios plotted in the theoretical HR diagram. The dot diameters are proportional to C/N with a largest value of 4.6 for B3-b1, 2.8 for Arcturus and 0.08 for Arp4203. Stars with [Fe/H] < −0.4 are plotted as filled dots and the more metal-rich ones as open circles.

with Meléndez et al. (2008) ($k = -0.6 \pm 0.15$). Our data are also marginally consistent with the data of Rich and Origlia (2005), which are confined to a narrow range in metallicity. The Cunha and Smith (2006) data set seems, however, to suggest a more shallow slope ($k = -0.1 \pm 0.2$).

In Figure 7 we plot the data points from the optical work by Fulbright et al. (2007), which also show an agreement in the slope ($k = -0.8 \pm 0.15$. In Figure 8 we plot the optical results from Zoccali et al. (2006), also presented in Lecureur et al. (2007) with a slope of $k = -0.6 \pm 0.15$, together with our determinations. Our results are similar to these in scatter and slope.

All our stars are in common with the optical analyses of Zoccali et al. (2006) but for one of them it was not possible to determine an oxygen abundance from the [O I] lines at 6300 Å. The metallicities and [O/Fe] for these stars from our and their analyses are given in Table 6. Note, that the stellar parameters are different in the two determinations. In Figure 8 we have marked and connected the two determination for the same stars. When comparing the two analyses, we see that the metallicities are within the uncertainties, marginally also for B6-b8 ($\Delta[\mathrm{Fe/H}]_{\mathrm{B6-b8}} = 0.13$ dex). The oxygen abundances generally agree within uncertainties, with the largest difference being $\Delta[\mathrm{O/Fe}]_{\mathrm{BW-f6}} = 0.18$ dex. However, our abundances may tend to be systematically lower. Given that our OH lines are very temperature sensitive, one reason for the differences could be that the effective temperatures are still not determined accurately enough. Another reason could be an overestimation of the line strengths in the optical spectra. Although the line strengths of the [OI] and the near-IR OH lines are comparable[5], the optical spectra used in Zoccali et al. (2006) reaches S/N~ 50 per resolution element, whereas our spectra have a S/N a factor of 2-4 larger and many more lines to use as oxygen criteria. Unknown blends might also affect the [OI] line.

Our [O/Fe] data suggest a high value of +0.4 up to [Fe/H]~ −0.3, after which the values decline rapidly with a slope of $k = -1.0 \pm 0.3$. This is the mean trend we have plotted in Fig. 3. A combination of our [O/Fe] data and those of Meléndez et al. (2008) (see Figure 2) corroborates our finding. This trend also fits well with the values found by Rich and Origlia (2005) (which are similar to those in Rich et al., 2007) and consistent with the trends found by Fulbright et al. (2007).

In all the three comparison Figures we have also plotted [O/Fe] vs. [Fe/H] for the thin and thick disks from Meléndez et al. (2008). When studying all [O/Fe] determinations in Figures 6 to 8, one gets the impression that these together may suggest similar, or possibly even higher values than those of the local thick disk of Meléndez et al. (2008). Note, that there may be important and different systematic errors in all these comparisons.

All trends seem to show a scatter that is similar or larger than the trends found for the thick and thin disks by Meléndez et al. (2008). This might, however, be expected for analyses of bulge stars since these are more difficult to anal-

[5] For example, for the giant B3-b8 the [OI] line has a strength of approximately $\log W_\lambda/\lambda = -5.1$ and the OH lines have line-strengths in the approximate range of $-5.7 < \log W_\lambda/\lambda < -5.0$

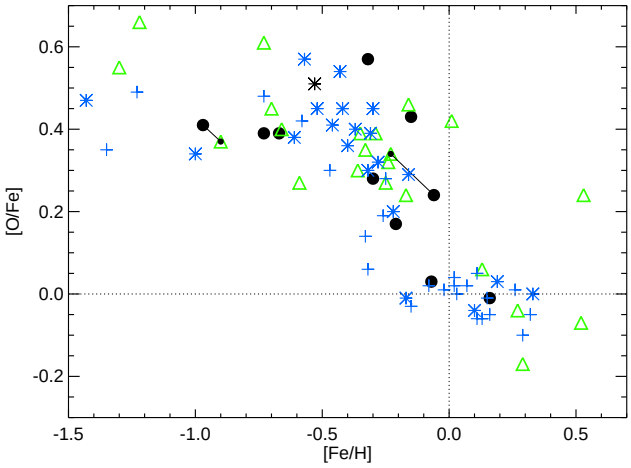

Fig. 7. Logarithmic ratios of oxygen to iron normalized on the solar value. Filled circles show our data from this paper, except that of Arp4203, and a black star indicates Arcturus at [Fe/H]= −0.53. Triangles show the optically determined values by Fulbright et al. (2007). The two small dots represent the stars from Fulbright et al. (2007) which were analysed by Ryde et al. (2009) from near-IR lines and which are reanalysed by us. The determinations by Fulbright et al. and our determinations are connected by full lines. The blue stars and plus signs represent thick disk and thin disk giants, respectively, from Meléndez et al. (2008).

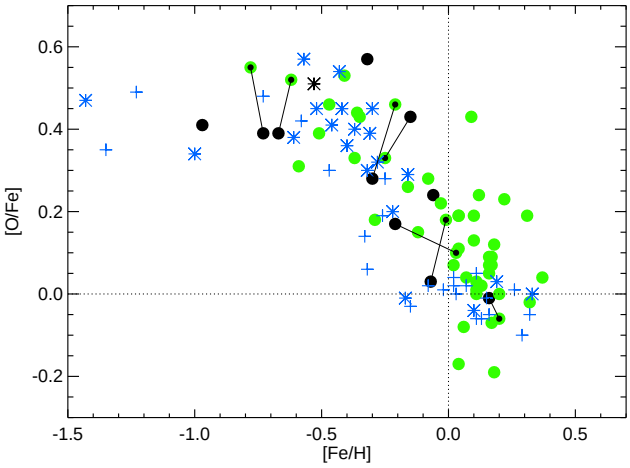

Fig. 8. Logarithmic ratios of oxygen to iron normalized on the solar value. Filled black circles show our data from this paper, except that of Arp4203, and a black star indicates Arcturus at [Fe/H]= −0.53. Filled green circles show the optically determined values by Lecureur et al. (2007) and Zoccali et al. (2006). The small black dots mark the stars from Lecureur et al. (2007) and Zoccali et al. (2006) for which we have determined the oxygen abundances from near-IR lines. These two determinations are connected. For the star B6-f7 there is only a near-IR determination of the oxygen abundance. When comparing these two determinations for the same stars, it should be noted that we have used new stellar parameters when determining the abundances from the near-IR spectra. The blue star and plus-sign symbols represent thick disk and thin disk giants, respectively, from Meléndez et al. (2008).

Table 6. [Fe/H] and [O/Fe] determined from near-IR lines in this paper and determinations based on optical lines (Lecureur et al., 2007; Zoccali et al., 2006), labelled L&Z.

Star	[Fe/H]	[O/Fe][a]	[Fe/H]$_{L\&Z}$	[O/Fe]$_{L\&Z}$
B3-b1	−0.73	0.39	−0.78	0.55
B3-b7	0.16	−0.01	0.20	−0.06
B3-b8	−0.67	0.39	−0.62	0.52
BW-b6	−0.15	0.43	−0.25	0.33
BW-f6	−0.30	0.28	−0.21	0.46
B6-f1	−0.070	0.030	−0.01	0.18
B6-b8	−0.10	0.10	+0.03	0.10
B6-f7	−0.32	0.57	−0.42	–

yse; our scatter reflects the expected uncertainties, and a cosmic scatter, if any, must be smaller than that.

5.1.2. Mg, Si, S, Ca, and Ti

We find that [Si, S/Fe]∼ +0.3 for metallicities up to at least [Fe/H]∼ −0.3 above which they seem to decline. Although Si and S may demonstrate slightly different trends, published abundance trends based on detailed abundance analyses for bulge stars all suggest that the ratio of α-element abundances relative to Fe show more or less enhanced values for all metallicities [Fe/H] < 0.0 (e.g. Carretta et al., 2001; Origlia et al., 2002; McWilliam and Rich, 2004; Origlia and Rich, 2004; Origlia et al., 2005a,b; Rich and Origlia, 2005; Cunha and Smith, 2006; Lecureur et al., 2007; Fulbright et al., 2007; Rich et al., 2007; McWilliam et al., 2008; Origlia et al., 2008). For instance, Lecureur et al. (2007) found high [α/Fe] ratios in the bulge as compared to the disks, which suggests an enrichment by mostly massive stars for all metallicities. Ryde et al. (2009) measured sulphur (a product of explosive nucleosynthesis) from near-IR spectra and found enhanced values. McWilliam and Rich (2004) demonstrated that Mg and Si are enhanced by 0.3 – 0.5 dex to super-solar metallicities. It should be noted here that our data do not support an enhanced [Si/Fe] and [S/Fe] values for [Fe/H> −0.3. The McWilliam and Rich (2004) [Ti/Fe] and [Ca/Fe] trends show a steeper decline than for Mg and Si with metallicity but not as much as for oxygen. In order to fit the different trends they suggest a skewed initial mass-function (IMF) with more massive stars in the bulge. Later, Fulbright et al. (2007) measured the abundances of O, Mg, Si, Ca, and Ti and found them all to decline in [α/Fe] as a function of metallicity but also that they retain higher values than those of the disks for all metallicities. Mg was found to be enhanced the most, while Si, Ca, and Ti (which are thought to be products from the explosive nucleosynthesis phase of Type II supernovae) follow each other well at lower enhancement levels. The large decline

of Si, Ca, and Ti compared to that of Mg was suggested to be caused by a metallicity-dependent decline of the former yields.

Our results for the α-elements do not support the existence of any significant "cosmic scatter" in the α-element abundances relative to iron in the bulge, but this is hardly conclusive since the observational scatter is considerable. Alves-Brito et al. (2009 in prep.) show, however, that their [α/Fe] ratio in both their bulge and thick disk giants have a scatter of only 0.03 dex. Also Fulbright et al. (2007) find in their mean [<SiCaTi>/Fe] a small scatter, much smaller than that of halo stars, and they interpret this as an indication that the bulge composition developed homogeneously, for example, due to efficient mixing.

5.1.3. The thick disk-bulge similarity

Fulbright et al. (2007), Lecureur et al. (2007) and Zoccali et al. (2006) find abundance trends, including those for oxygen, that are different between the thick disk dwarfs and turn-off stars measured by Bensby et al. (2004) and Reddy et al. (2005) and bulge giants as measured from their own optical spectra. In contrast, Meléndez et al. (2008), by means of a homogeneous analysis of near-IR spectra of bulge and disk giants, find no chemical distinction between the local thick disk (up to [Fe/H]~ -0.2) and the bulge, suggesting that the two populations show a similar chemical evolution and that the star-formation rates would not be significantly different. As shown in Figures 6 to 8, the abundances measured here for bulge giants are consistent, within the uncertainties, with previous ones, both optical and near-IR. In the comparison with the thick disk, we follow the approach of Meléndez et al, restricting the comparison to giants in both components, measured in a fully consistent way. Our bulge stars have abundances similar to those of thick disk giants.

5.2. The carbon and nitrogen abundances

Estimates from the optical wavelength region of the carbon and nitrogen abundances are highly uncertain (in many cases only upper limits are known), whereas the CO, CN, and OH lines in the near-IR together easily provide them. The C and N abundances might give clues to, for instance, the importance of W-R winds and the evolutionary state of the giants, thereby indicating whether the measured oxygen abundances are the original, unprocessed ones.

5.2.1. First dredge-up and the measured oxygen abundance

Low-mass giants that have ascended the giant branch for the first time have only experienced the first dredge-up of CN-processed material from the interior. Thus, the CN cycle's products, which are mainly ^{14}N and some ^{13}C converted from ^{12}C, are dredged-up to their surfaces. This is expected not to alter the sum of the number of carbon and nitrogen nuclei, while the measured oxygen abundances should reflect the original abundances in the giants. From Table 5 we see that all stars (with the exception of Arp4203) only show signs of the first dredge-up and thus no further processing of oxygen through the NO cycle, nor any increase in the C abundance characteristic of the third dredge-up on the Asymptotic Giant Branch.

The galactic chemical evolution of carbon and nitrogen are still somewhat uncertain. Bensby and Feltzing (2006) find a constant [C/Fe] close to +0.1 for -0.9 <[Fe/H]< 0.0 for disk stars and the summarized observational trend of [N/Fe] vs. [Fe/H] as presented in Goswami and Prantzos (2000) is constant at a solar value. Thus, if the (C+N) abundances are expected to follow that of iron, one would expect the [(C+N)/Fe] to be slightly below +0.1 for all metallicities in the Galactic disk, which is consistent with what we find. If the atmospheres of our stars had also been exposed to ON-cycled material (in which ^{16}O is converted to ^{14}N), their nitrogen abundances would have been larger (resulting in larger [(C+N)/Fe] ratios and a larger scatter) with an accompanying lower oxygen abundance. It therefore seems likely that our measured oxygen abundances can be taken as the stars original unprocessed abundance. This is also what is to be expected if the stars have relatively low masses, and are still in the H-shell burning or He-core burning phase, i.e. are on their first ascent along the giant branch or are clump stars.

5.2.2. The role of W-R stars

The oxygen abundance trends found from optical spectra of K giants in the bulge by McWilliam and Rich (2004), indicate a surprising interruption of oxygen production in the bulge for high metallicities. The decrease in oxygen abundance is consistent with the strange scenario of no oxygen production for [Fe/H] > -0.5. McWilliam and Rich (2004) suggest that this could be connected to the onset of the Wolf-Rayet (W-R) phenomenon, which would be vital for the production of the CNO elements. Carbon is lost in metallicity-sensitive, radiation-driven stellar winds of metal-rich W-Rs preventing carbon to be converted into oxygen, thereby reducing the oxygen production. Hence, the steep oxygen decline would not be specific for the stellar population(s) in the bulge, but a metal-dependent phenomenon with metallicity-sensitive stellar yields from massive stars playing an important role. Indeed, McWilliam et al. (2008) show that the Galactic bulge and the thin disk experience the same decline in [O/Mg] versus [Mg/H] diagram, supporting this hypothesis (or the alternative hypothesis that IMF is considerably metallicity dependent), since both oxygen and magnesium are synthesised in the hydrostatic cores of massive stars in a similar fashion. In such a diagram the effects of the Fe-producing Type Ia supernovae are eliminated. The decline in the [O/Fe] vs. [Fe/H] plot in the bulge would also reflect the decrease in oxygen yields due to W-R stars, and not only the onset of Fe production from Type Ia supernovae. The latter gives clues to the timescales of the rates and duration of the star formation in the early bulge. Similarly, Fulbright et al. (2007) also relate their low oxygen over-abundances to lower oxygen yields at higher metallicities, due to metallicity-dependent W-R winds. This finds support in the calculations for rotating massive star models by Meynet and Maeder (2005) who conclude that higher C/O abundances are to be expected from high-

metallicity WR stars. This idea is strengthened by Cunha et al. (2008) who derive Fluorine (^{19}F) abundances for a sample of bulge stars. Their results suggest that winds from metal-rich W-R stars contribute more to the production of this element than do the AGB stars in the bulge compared to the situation in the disk.

If the W-R hypothesis, invoked to explain the steeper decline of the [O/Fe] ratio as compared to the other α elements is correct, it could mean a dramatic increase of the carbon yields and thereby of the carbon abundances versus metallicity, since the carbon lost from the star is material that would otherwise be expected to be transformed to oxygen in later stages and then expelled by supernovae explosions. However, it is fully conceivable that much of matter, lost in the W-R stage, which would else be transformed to oxygen, is primarily as yet helium. More detailed model calculations are needed to explore which C enrichment is to be expected. The mass loss in massive stars would anyhow have a large impact on the formation of carbon and oxygen, especially in metal-rich populations. The carbon versus metallicity trend is therefore a crucial test of the W-R scenario. However, assuming that nitrogen is not affected we do not trace a dramatic increased carbon production from our data. The [(C+N)/Fe] ratio we find has a mean of $+0.08 \pm 0.09$ dex, and the [(C+N)/Fe] vs. [Fe/H] shows a modest, if any, slope of $k = \frac{\partial[(\mathrm{C+N})/\mathrm{Fe}]}{\partial[\mathrm{Fe/H}]} = +0.07 \pm 0.09$. Thus, our data do not give any strong further support to this hypothesis.

6. Conclusions

Abundance determinations for stars are known to be plagued by systematic errors that may be difficult to estimate. In order to discuss the properties of different stellar populations, homogeneous differential spectroscopic studies, and detailed comparisons of results of different studies, are significant. In the present study we have tried to follow this route, and find a satisfactory agreement with results obtained in the optical, as well as IR, when a common temperature scale is used for the stars. With our high-resolution IR spectroscopy, we have explored the CNO abundances, as well as the abundances of Si, S, Ti and Fe, for 11 bulge giants. We have found enhanced [O/Fe], [Si/Fe], and [S/Fe] values with increasing [Fe/H] up to approximately [Fe/H]~ -0.3, after which these abundance ratios relative to Fe decrease. This suggests an early and rapid star formation in the bulge. Our investigation is not devised to make a detailed comparison with thick disk stars and determine the relationship between these two populations; such a study should be made differentially to minimise systematic uncertainties. Our abundance trends are, however, consistent with a similarity between these populations as was found in the differential study by Meléndez et al. (2008). Such a similarity suggests that the picture of an isolated classical bulge may be oversimplified. Inner-disk stars, at smaller galactocentric distances, should be explored in order to deepen the understanding of a possible physical connection between the bulge and the thick disk.

From our C and N abundances we conclude that our stars are first-ascent red-giants or clump stars, suggesting that their oxygen abundances are not affected by CNO cycling. Furthermore, we find that there is no significant increase in the carbon abundances for high metallicities, which could have been expected if W-R stars were to explain the large decline in [O/Fe] vs. metallicity.

We have demonstrated that for the same stars several different determinations of the stellar parameters from optical spectra produce significantly different results, implying important systematic uncertainties. Attempts to reduce these should be made. Note also that Chiappini et al. (2009) compare, among others, the oxygen abundances derived from planetary nebulae (PNe) and giants in the bulge and find that the abundances determined from giant star spectra are systematically higher by 0.3 dex. They conclude that this discrepancy may be caused by systematic uncertainties in either the PNe or giant star abundance determinations, or both.

To fully clarify the situation of the origin and evolution of the galactic bulge, additional near-IR abundance surveys of elements (especially more α elements) are needed. Most earlier investigations have been restricted to Baade's window. Different regions of the bulge are now being explored, and further systematic such work is needed.

Table 7. Line list of metal lines with astrophysical oscillator strengths, see text. (1) The wavelength in air, (2) the excitation energy of the lower level, (3) $\log gf$, (4) the radiation damping parameter (when no value was available the very small value of 1.00×10^5 was used), (5) the van der Waals damping marked with an 'A' when calculated according to Anstee and O'Mara (1995), Barklem et al. (2000) and references therein, or Barklem P., private communication (if a number is instead given this is an empirical correction factor to the van der Waals damping computed according to Unsöld (1955)). (6) a star '*' when the $\log gf$ value was determined from fits to the spectrum of Arcturus rather than from the solar spectrum.

Wavelength [Å]	$\chi_{\rm exc}$ [eV]	$\log gf$	$\Gamma_{\rm rad}$ [rad s^{-1}]	van der Waal	Arcturus fit
Si I					
15330.191	6.718	−1.90	1.00E+05	A	
15338.780	6.261	−2.58	1.00E+05	A	
15342.973	7.108	−1.85	1.00E+05	A	*
15361.160	5.954	−2.12	1.00E+05	A	
15375.430	6.734	−1.53	1.00E+05	A	
15376.830	6.223	−0.66	1.00E+05	A	
15376.830	6.721	−1.13	1.00E+05	A	
15381.738	6.721	−2.03	1.00E+05	A	
15387.069	7.166	−1.64	1.00E+05	A	*
15471.964	6.726	−2.40	1.00E+05	A	
15496.964	7.006	−2.54	1.00E+05	1.30	
15506.980	6.727	−1.55	1.00E+05	A	
15520.115	7.108	−1.85	1.00E+05	A	*
15532.449	6.718	−2.18	1.00E+05	A	
15538.463	6.761	−2.36	1.00E+05	A	*
15557.790	5.964	−0.65	1.00E+05	A	
15561.251	7.040	−1.23	1.00E+05	A	
15638.472	6.734	−1.93	1.00E+05	A	
15674.653	7.064	−1.30	1.00E+05	A	
S I					
15400.060	8.700	0.40	1.00E+05	A	
15403.770	8.700	0.40	1.00E+05	A	
15405.979	8.700	−1.45	1.00E+05	A	
15422.260	8.701	0.55	1.00E+05	A	
15422.260	8.701	−0.62	1.00E+05	A	
15469.820	8.045	−0.45	1.00E+05	A	
15475.620	8.046	−0.75	1.00E+05	A	
15478.480	8.046	−0.10	1.00E+05	A	
Ti I					
15334.840	1.887	−1.05	2.93E+06	A	
15381.110	2.333	−2.29	7.13E+07	A	*
15399.285	2.334	−2.00	7.13E+07	A	*
15426.970	1.873	−2.52	2.76E+06	A	*
15543.780	1.879	−1.15	2.76E+06	A	
15602.840	2.267	−1.60	2.31E+06	A	
15698.979	1.887	−2.14	2.76E+06	A	*
Cr I					
15680.081	4.697	0.10	2.04E+08	A	
Mn I					
15673.385	5.133	−0.57	6.68E+07	A	
Fe I					
15323.550	6.350	−0.99	1.00E+05	A	
15335.380	5.410	0.00	1.12E+08	A	
15343.810	5.653	−0.70	1.16E+08	A	
15348.398	5.874	−1.70	9.18E+07	A	
15348.950	5.950	−1.00	1.00E+05	A	
15360.230	4.260	−2.97	8.75E+06	A	
15381.980	3.640	−3.03	1.00E+05	A	

Table 7. continued.

Wavelength [Å]	$\chi_{\rm exc}$ [eV]	$\log gf$	$\Gamma_{\rm rad}$ [rad s^{-1}]	van der Waal	Arcturus fit
15394.670	5.621	−0.03	1.61E+08	A	
15395.720	5.621	−0.23	1.21E+08	A	
15451.330	6.450	−0.48	1.00E+05	A	
15475.923	5.874	−2.00	1.26E+08	A	
15485.450	6.280	−0.93	1.00E+05	A	
15490.340	2.198	−4.85	1.14E+04	1.40	
15490.880	6.290	−0.57	1.00E+05	A	
15493.515	6.368	−1.45	2.34E+08	A	
15493.550	6.450	−1.25	1.00E+05	A	
15496.690	6.290	−0.30	1.00E+05	A	
15499.410	6.350	−0.32	1.00E+05	A	
15500.800	6.320	−0.12	1.00E+05	A	
15501.320	6.290	0.10	1.00E+05	A	
15502.170	6.350	−1.07	1.00E+05	A	
15514.280	6.290	−0.75	1.00E+05	A	
15522.640	6.320	−0.97	1.00E+05	A	
15524.543	5.793	−2.15	2.55E+08	A	
15531.750	5.642	−0.48	1.22E+08	A	
15534.260	5.642	−0.30	1.21E+08	A	
15537.690	6.320	−0.50	1.71E+08	A	
15554.510	6.280	−1.20	1.00E+05	A	
15560.780	6.350	−0.51	1.00E+05	A	
15566.725	6.350	−0.53	1.71E+08	A	
15579.080	6.320	−1.05	1.00E+05	A	
15588.260	5.490	−2.70	1.00E+05	A	
15588.260	6.370	0.34	1.00E+05	A	
15590.050	6.240	−0.43	1.00E+05	A	
15593.740	5.033	−1.92	5.96E+08	A	
15604.220	6.240	0.49	1.00E+05	A	
15611.150	3.415	−3.12	1.57E+07	A	
15614.100	6.350	−0.42	1.00E+05	A	
15621.664	5.539	0.42	1.12E+08	A	
15629.630	4.559	−3.08	2.72E+08	A	
15631.112	3.642	−4.10	8.04E+07	A	
15631.950	5.352	0.15	1.14E+08	A	
15637.965	6.361	−2.20	2.33E+08	A	
15638.919	5.814	−1.74	1.41E+08	A	
15639.480	6.410	−0.88	1.00E+05	A	
15645.010	6.310	−0.57	1.00E+05	A	
15647.410	6.330	−1.05	1.00E+05	A	
15648.535	5.426	−0.66	1.12E+08	A	
15652.870	6.250	−0.13	1.00E+05	A	
15656.669	5.874	−1.80	1.41E+08	A	
15662.010	5.830	0.25	1.00E+05	A	
15662.320	6.330	−0.80	1.00E+05	A	
15670.130	6.200	−1.02	1.00E+05	A	
15671.000	6.330	−0.57	1.00E+05	A	
15671.860	5.920	−1.40	1.00E+05	A	
15673.150	6.250	−0.73	1.00E+05	A	
15676.599	5.106	−1.85	8.13E+07	A	
15677.520	6.250	0.20	1.00E+05	A	
15682.510	6.370	−0.40	1.00E+05	A	
15686.020	6.330	−0.20	1.00E+05	A	
15686.440	6.250	0.17	1.00E+05	A	
15691.850	6.250	0.61	1.00E+05	A	

Table 7. continued.

Wavelength [Å]	$\chi_{\rm exc}$ [eV]	$\log gf$	$\Gamma_{\rm rad}$ [rad s^{-1}]	van der Waal	Arcturus fit
15692.750	5.385	−0.50	1.14E+08	A	
Ni I					
15555.370	5.488	0.13	1.48E+08	A	
15556.016	5.283	−3.15	1.68E+08	A	
15605.680	5.300	−0.47	1.00E+05	A	
15605.680	5.300	−0.96	1.00E+05	A	
15632.654	5.305	−0.01	9.71E+07	A	

Acknowledgements. N.R. is a Royal Swedish Academy of Sciences Research Fellow supported by a grant from the Knut and Alice Wallenberg Foundation. Funds from Kungl. Fysiografiska Sällskapet i Lund are acknowledged. NR, BE, and BG acknowledge support from the Swedish Research Council, VR. JM acknowledge support from the Portuguese FCT (PTDC/CTE-AST/65971/2006, Ciencia 2007). MZ and DM are supported by FONDAP Center for Astrophysics 15010003, by BASAL CATA PFB 0609, and by FONDECYT. Kjell Eriksson is thanked for valuable help and discussions concerning the running of the MARCS programme. The referee is thanked for valuable suggestions.

References

Anstee, S. D. and O'Mara, B. J., 1995, MNRAS 276, 859
Ballester, P., Banse, K., Castro, S., et al., 2006, in Society of Photo-Optical Instrumentation Engineers (SPIE) Conference Series, Vol. 6270 of Presented at the Society of Photo-Optical Instrumentation Engineers (SPIE) Conference
Barklem, P. S., Piskunov, N., and O'Mara, B. J., 2000, A&AS 142, 467
Bensby, T. and Feltzing, S., 2006, MNRAS 367, 1181
Bensby, T., Feltzing, S., and Lundström, I., 2004, A&A 415, 155
Bensby, T., Feltzing, S., Lundström, I., and Ilyin, I., 2005, A&A 433, 185
Bournaud, F. and Elmegreen, B. G., 2009, ApJ 694, L158
Carollo, C. M., Scarlata, C., Stiavelli, M., Wyse, R. F. G., and Mayer, L., 2007, ApJ 658, 960
Carretta, E., Cohen, J. G., Gratton, R. G., and Behr, B. B., 2001, AJ 122, 1469
Chiappini, C., Górny, S. K., Stasińska, G., and Barbuy, B., 2009, A&A 494, 591
Clarkson, W., Sahu, K., Anderson, J., et al., 2008, ApJ 684, 1110
Cunha, K. and Smith, V. V., 2006, ApJ 651, 491
Cunha, K., Smith, V. V., and Gibson, B. K., 2008, ApJ 679, L17
da Silva, L., Girardi, L., Pasquini, L., et al., 2006, A&A 458, 609
Elmegreen, B. G. and Elmegreen, D. M., 2005, ApJ 627, 632
Förster Schreiber, N. M., Genzel, R., Bouche, N., et al., 2009, ArXiv e-prints
Fulbright, J. P., McWilliam, A., and Rich, R. M., 2006, ApJ 636, 821
Fulbright, J. P., McWilliam, A., and Rich, R. M., 2007, ApJ 661, 1152
Genzel, R., Burkert, A., Bouché, N., et al., 2008, ApJ 687, 59
Genzel, R., Tacconi, L. J., Eisenhauer, F., et al., 2006, Nature 442, 786
Goldman, A., Schoenfeld, W., Goorvitch, D., et al., 1998, JQSRT 59, 453
Goorvitch, D., 1994, ApJSS 95, 535
Goswami, A. and Prantzos, N., 2000, A&A 359, 191
Gray, D. F., 1992, The observation and analysis of stellar photospheres, Cambridge ; New York : Cambridge University Press, 1992. 2nd ed.
Gustafsson, B., Edvardsson, B., Eriksson, K., et al., 2008, A&A 486, 951
Hekker, S. and Meléndez, J., 2007, A&A 475, 1003
Hinkle, K., Wallace, L., and Livingston, W., 1995a, PASP 107, 1042
Hinkle, K., Wallace, L., and Livingston, W. C., 1995b, Infrared atlas of the Arcturus spectrum, 0.9-5.3 microns, San Francisco, Calif. : Astronomical Society of the Pacific, 1995.
Hinkle, K. H., Cuberly, R. W., Gaughan, N. A., et al., 1998, SPIE 3354, 810
Immeli, A., Samland, M., Gerhard, O., and Westera, P., 2004, A&A 413, 547
Jørgensen, U. G. and Larsson, M., 1990, A&A 238, 424
Jørgensen, U. G., Larsson, M., A., I., and Yu, B., 1996, A&A 315, 204
Käufl, H. U., Amico, P., Ballester, P., et al., 2006, The Messenger 126, 32
Käufl, H.-U., Ballester, P., Biereichel, P., et al., 2004, in A. F. M. Moorwood and M. Iye (eds.), Society of Photo-Optical Instrumentation Engineers (SPIE) Conference Series, Vol. 5492 of Presented at the Society of Photo-Optical Instrumentation Engineers (SPIE) Conference, pp 1218–1227

Kerber, F., Bristow, P., and Rosa, M. R., 2008a, in Society of Photo-Optical Instrumentation Engineers (SPIE) Conference Series, Vol. 7014 of Presented at the Society of Photo-Optical Instrumentation Engineers (SPIE) Conference
Kerber, F., Nave, G., and Sansonetti, C. J., 2008b, ApJS 178, 374
Kormendy, J. and Kennicutt, Jr., R. C., 2004, ARA&A 42, 603
Langhoff, S. R. and Bauschlicher, C. W., 1993, Chem. Phys. Letters 211, 305
Lecureur, A., 2007, Ph.D. thesis, GEPI, Observatoire de Paris, CNRS, Université Paris Diderot; Place Jules Janssen, 92190 Meudon, France
Lecureur, A., Hill, V., Zoccali, et al., A., 2007, A&A 465, 799
Livingston, W. and Wallace, L., 1991, An atlas of the solar spectrum in the infrared from 1850 to 9000 cm-1 (1.1 to 5.4 micrometer), NSO Technical Report, Tucson: National Solar Observatory, National Optical Astronomy Observatory, 1991
Matteucci, F. and Romano, D., 1999, Ap&SS 265, 311
McWilliam, A., Matteucci, F., Ballero, S., Rich, R. M., Fulbright, J. P., and Cescutti, G., 2008, AJ 136, 367
McWilliam, A. and Rich, R. M., 2004, in A. McWilliam and M. Rauch (eds.), Origin and Evolution of the Elements
Meléndez, J., Asplund, M., Alves-Brito, A., et al., 2008, A&A 484, L21
Meléndez, J. and Barbuy, B., 1999, ApJS 124, 527
Meynet, G. and Maeder, A., 2005, A&A 429, 581
Moorwood, A., 2005, in H. U. Käufl, R. Siebenmorgen, and A. F. M. Moorwood (eds.), High Resolution Infrared Spectroscopy in Astronomy, p. 15
Origlia, L. and Rich, R. M., 2004, AJ 127, 3422
Origlia, L., Rich, R. M., and Castro, S., 2002, AJ 123, 1559
Origlia, L., Valenti, E., and Rich, R. M., 2005a, MNRAS 356, 1276
Origlia, L., Valenti, E., and Rich, R. M., 2008, MNRAS 388, 1419
Origlia, L., Valenti, E., Rich, R. M., and Ferraro, F. R., 2005b, MNRAS 363, 897
Ortolani, S., Renzini, A., Gilmozzi, R., et al., 1995, Nature 377, 701
Paufique, J., Biereichel, P., Delabre, B., et al., 2006, in Society of Photo-Optical Instrumentation Engineers (SPIE) Conference Series, Vol. 6272 of Society of Photo-Optical Instrumentation Engineers (SPIE) Conference Series
Piskunov, N. E., Kupka, F., Ryabchikova, T. A., Weiss, W. W., and Jeffery, C. S., 1995, A&AS 112, 525
Querci, F., Querci, M., and Kunde, V., 1971, A&A 15, 256
Ramírez, I. and Meléndez, J., 2005a, ApJ 626, 446
Ramírez, I. and Meléndez, J., 2005b, ApJ 626, 465
Reddy, B. E., Lambert, D. L., and Allende Prieto, C., 2006, MNRAS 367, 1329
Reid, M. J., 1993, ARA&A 31, 345
Renzini, A., 2006, ARA&A 44, 141
Rich, R. M. and Origlia, L., 2005, ApJ 634, 1293
Rich, R. M., Origlia, L., and Valenti, E., 2007, ApJ 665, L119
Ryde, N., Edvardsson, B., Gustafsson, B., et al., 2009, A&A 496, 701
Santos, N. C., Lovis, C., Pace, G., Meléndez, J., and Naef, D., 2009, A&A 493, 309
Silk, J. and Wyse, R. F. G., 1993, Phys. Rep. 231, 293
Stetson, P. B. and Pancino, E., 2008, PASP 120, 1332
Tody, D., 1993, in R. J. Hanisch, R. J. V. Brissenden, and J. Barnes (eds.), ASP Conf. Ser. 52: Astronomical Data Analysis Software and Systems II, p. 173
Unsöld, A., 1955, Physik der Sternatmospharen, MIT besonderer Berucksichtigung der Sonne., Berlin, Springer, 1955. 2. Aufl.
Zoccali, M., Hill, V., Lecureur, A., et al., 2008, A&A 486, 177
Zoccali, M., Lecureur, A., Barbuy, B., et al. 2006, A&A 457, L1
Zoccali, M., Renzini, A., Ortolani, S., et al., 2003, A&A 399, 931